Facultad de Ciencias
Universidad Zaragoza

Development of nanostructured carbon-based catalysts for photocatalytic conversion of CO_2 into added-value fuels

Author

Yi Cai

Director

Francisco Balas Nieto

Master in

Nanostructured Material for Nanotechnology Applications

2019/2020

Development of nanostructured carbon-based catalysts for photocatalytic conversion of CO_2 into added-value fuels

Yi Cai

Abstract

Nowadays, energy shortages, carbon resource shortages, and global warming are the major challengs. The usage of photocatalysis to realize the conversion of CO_2 into added-value fuels can alleviate the above problems. As a visible light photocatalyst without metal components, g-C_3N_4 has unique electronic structure, high catalytic activity, good chemical and thermal stability, which has caused wide attention. This article mainly summarized the basic properties and structure of g-C_3N_4. Besides, we introduced the commonly used preparation methods and modification methods of g-C_3N_4, and prospects the application of g-C_3N_4.

Keywords: g-C_3N_4; photocatalysis; CO_2 reduction

INDEX

1 Introduction

Carbon dioxide (CO_2) is the main greenhouse gas in the atmosphere, and the increasing concentration of CO_2 is one of the most serious problems which contribute to global warming and climate change. Due to the development of industry and society, carbon dioxide emissions mainly come from the burning of fossil fuels in energy use. As the demand for fossil resources continues to grow in the coming decades, it is essential to reduce carbon dioxide emission.

The main ways to reduce carbon dioxide can be divided into emission reduction and post-treatment. The post-treatment of carbon dioxide can be further divided into deep sea burial, chemical adsorption storage and chemical conversion. Compared with traditional, high-energy-consuming methods such as capture or geological storage, the resource utilization of CO_2 is a more promising approach which can simultaneously alleviate the greenhouse effect and energy crisis. Various approaches have been developed in basic research, such as thermal catalysis, photocatalysis, electrocatalysis, photo-electric synergistic catalysis and organic catalytic conversion, to convert CO_2 molecules into high value-added chemicals.

Among them, CO_2 conversion driven by solar energy is an environmentally friendly treatment method which has outstanding advantages such as mild reaction conditions and so on. The photocatalytic reduction of CO_2 is similar to the photosynthesis of plants in nature. It takes the greenhouse gas CO_2 emitted by humans and the abundant water resources on the earth as raw materials. Then CO_2 is reduced to various energy-containing reducing products through the action of light energy. It is consumed by the existing forms of energy utilization again, and finally completes the carbon cycle process, realizing the balanced development of energy demand for human development and sustainable use of environmental resources.

2 Photocatalytic reduction of CO_2

Inspired by photosynthesis, solar energy is used to produce hydrocarbons and O_2 from CO_2 and H_2O. In this process, energy can be simultaneously generated when CO_2 in the atmosphere can be reduced. Therefore, photocatalytic reduction of CO_2 is

the most important way in artificial photosynthesis.

2.1 Basic principles and reaction mechanism

When the photocatalyst is excited by radiant light, the generated charge carriers will migrate to the surface of the photocatalyst and interact with the CO_2 molecules adsorbed on the surface. The principle of photocatalytic reduction of CO_2 is shown in **Fig 1**[1]. In particular, the reaction of photocatalytic reduction of CO_2 includes CO_2 reduction and H_2O oxidation, involving the cleavage of C=O bonds and the formation of C-H bonds. Therefore, the photoreduction of CO_2 is not a single-electron reaction process, but a proton-induced multi-electron reaction to produce various products, including the following processes:

$$CO_2 + 2H^+ + 2e^- \rightarrow HCOOH \quad E_{redox} = -0.20\ V \quad (1)$$

$$CO_2 + 2H^+ + 2e^- \rightarrow CO + H_2O \quad E_{redox} = -0.12\ V \quad (2)$$

$$CO_2 + 4H^+ + 4e^- \rightarrow HCHO + H_2O \quad E_{redox} = -0.07\ V \quad (3)$$

$$CO_2 + 6H^+ + 6e^- \rightarrow CH_3OH + H_2O \quad E_{redox} = +0.03\ V \quad (4)$$

$$CO_2 + 8H^+ + 8e^- \rightarrow CH_4 + 2H_2O \quad E_{redox} = +0.17\ V \quad (5)$$

Thermodynamically, CO_2 is an extremely stable molecule. The dissociation energy of the C=O double bond is as high as 750 $kJ \cdot mol^{-1}$, which is significantly higher than the C-H bond (430 $kJ \cdot mol^{-1}$) and C-C bond (336 $kJ \cdot mol^{-1}$) in the reduction product, which means that a large amount of energy needs to be injected into the system to trigger the activation and conversion process of CO_2. At the same time, the C (Ⅳ) is in the highest oxidation state in the CO_2 molecule, and various products can be obtained according to the number of electrons obtained in the reaction. In the photocatalytic reaction, CO_2 can usually be reduced to carbon monoxide (CO), methane (CH_4), formic acid (HCOOH) or ethanol (CH_3OH) and other substances, which with the side reaction of water reduction to generate hydrogen, and it will be significantly reduced the selectivity of the target product.

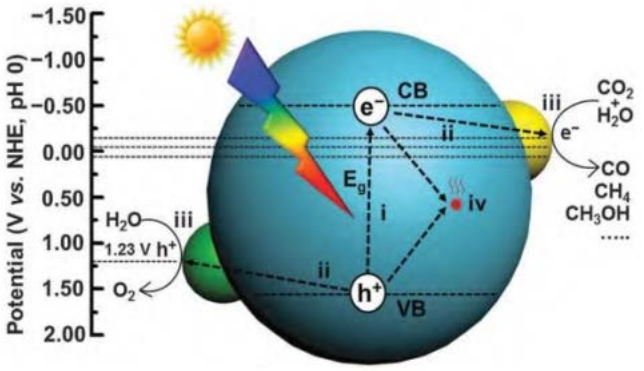

Fig. 1. Schematic illustration of reaction steps in photocatalytic CO_2 reduction with H_2O

From the current research status, the photoreduction of CO_2 still faces the difficulties of low conversion rate and poor selectivity. In order to obtain a higher efficiency, the catalyst not only needs to have a suitable energy band structure, but also needs to optimize its surface structure and electronic structure to improve the ability of catalyst to adsorb and activate CO_2 which could inhibit the formation of by-products. Therefore, how to overcome these obstacles has become an important issue in the design of efficient photocatalysts for CO_2 photocatalytic reduction.

2.2 Application of carbon-based photocatalytic catalysts in CO_2 reduction

There are many kinds of photocatalysts which can be used in the photoreduction of CO_2. They can be divided into metal and non-metal photocatalysts. The former includes oxides, sulfides, bismuth oxyhalides (BiOX), metal organic framework compounds (MOFs) and so on. The latter mainly includes carbon-based catalysts and *h*-BN. This article will focus on the specific introduction of carbon-based catalysts and examples of their realization of the photocatalytic conversion of CO_2.

2.2.1 Graphene and its derivatives

Graphene and its derivatives (GO, rGO) are a well-known catalyst. Since graphene was first reported in 2004, it has been widely used in many research fields due to its excellent mechanical, thermal, optical and electronic properties. As shown in **Fig 2**[2], the use of graphene-based materials for CO_2 photoreduction shows the following advantages: (1) Ultra-thin 2D morphology gives graphene a high specific

surface area and provides abundant adsorption sites for the reaction substrate. (2) Graphene is a zero band gap material with excellent conductivity and electron mobility. (3) It can form π-π conjugate with CO_2 molecules to promote CO_2 activation. Zou[3] obtained a TiO_2/graphene composite material rich in Ti^{3+} sites by using the simultaneous reduction-hydrolysis technology. The abundant Ti^{3+} in TiO_2 particles can capture photogenerated electrons to inhibit recombination, and synergize with graphene for photocatalytic reaction to achieve CO_2 reduction and coupling to generate CH_4 and C_2H_6.

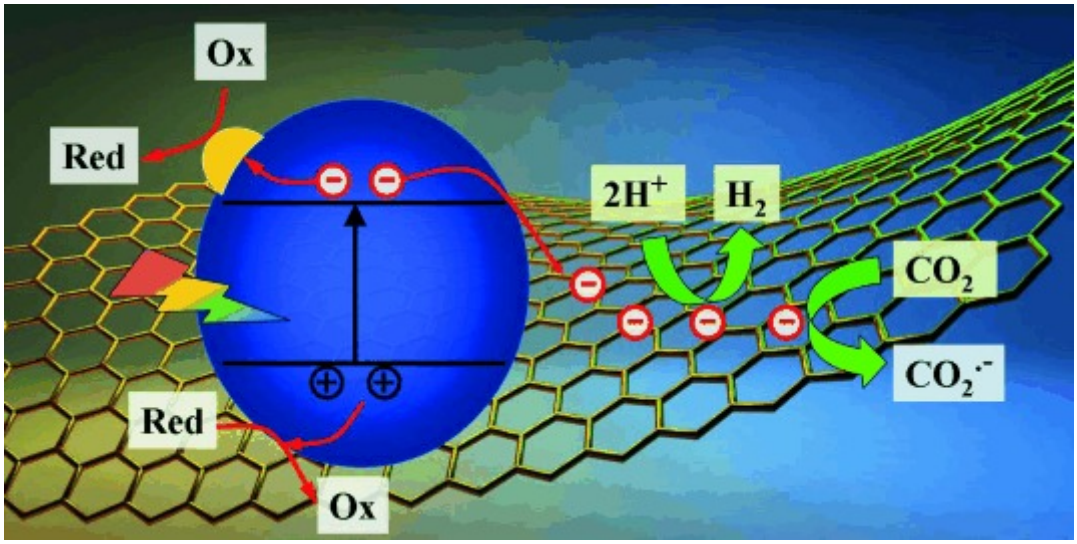

Fig.2. Graphene-based photocatalysts for CO_2 photoreduction.

2.2.2 GDY

Graphene (GDY) is an allotrope of graphene. It is a 2D planar structure composed of sp- and sp^2-hybrid carbon, with a band gap ranging from 0.46 to 1.22 eV[4]. In terms of electrical properties, GDY has a moderate band gap and high electron mobility (104~105 $cm^2 \cdot V^{-1} \cdot s^{-1}$). The abundant C≡C makes the electron conjugation degree of GDY high, which is very beneficial to the adsorption and activation of CO_2. From the structural point of view, GDY contains periodic arrangement of triangular holes, which can effectively reduce its density[4-5]. Due to the many uncontrollable factors in the reaction of preparing 2D GDY, including monomer stability, side reactions, monomer orientation coupling[6], low yield, etc., there are only a few literature reports[7] about the use of 2D GDY in CO_2 photoreduction reactions.

2.2.3 g-C_3N_4

g-C_3N_4 is a new type of non-metallic semiconducting polymer material. It consists of C and N atoms through sp^2-hybridization to form a large π conjugated system with a high degree of delocalization, generally composed of anti-triazine ring structural which has a larger binding energy and more stable. Most of the literature usually uses N-rich molecules such as urea, cyanamide and melamine as precursors to form g-C_3N_4 at high temperatures[8]. It has more suitable Eg (≈2.77 eV) and CB positions (≈-1 V). At the same time, the spectral absorption covering the ultraviolet and visible regions can meet the needs of CO_2 reduction.

3 Advantages and challenges of g-C_3N_4 catalyst

In recent years, g-C_3N_4 has become a popular material in the field of photocatalysis due to its special energy band structure and easy manufacturing advantages. It can be excited by visible light irradiation, so it has great potential value for the utilization and conversion of solar energy; due to the existence of quantum confinement effect, the position of CB of g-C_3N_4 moves up slightly, and the reduction ability is further enhanced. It forms π-π conjugation with CO_2, which significantly promotes the adsorption and activation of CO_2. However, g-C_3N_4 catalyst still has some bottlenecks that limit its photocatalytic activity, such as high photo-generated electron-hole pair recombination efficiency, limited surface catalytic reaction active sites and low specific surface area. But most importantly, g-C_3N_4 is a very ideal modification platform, and its performance can be optimized by controlling the preparation method of the material, as well as the doping, compounding, defect construction, surface functional group control and other ways.

4 g-C_3N_4 catalyst and the effect of its preparation method g-C_3N_4 on performance

In recent years, some new properties of g-C_3N_4 have been gradually discovered by scientific researchers, which has further promoted the upsurge of research on g-C_3N_4 semiconductor materials. So far, g-C_3N_4 with a variety of morphologies has been successfully synthesized, including nanofibers, nanotubes, nanosheets, spheres, etc. These studies have strongly promoted the deep development of g-C_3N_4 in the

field of photocatalysis. Using nitrogen-containing organic molecules as precursors, it is the simplest and direct method to prepare g-C_3N_4 materials under high temperature (500~600 ℃) pyrolysis polymerization in air or inert atmosphere. However, g-C_3N_4 prepared by this method had shortcomings such as low specific surface area, which greatly limits its application in the field of catalysis. In comparison, the template method is currently the main method for preparing g-C_3N_4 with high specific surface area and large pore size. According to the type of template used, it can be divided into hard template method, soft template method and no template method.

4.1 Hard-templating method

The hard-templating method is used to design and prepare g-C_3N_4 materials with various structures and morphologies ranging from millimeters to nanometers. The introduction of different morphologies and highly regular pore structures can effectively adjust the structural properties and surface interaction of g-C_3N_4[9-10], promoting the mass transfer and diffusion process of the catalyst surface, helping optimize its semiconductor energy band structure and light absorption characteristics, and improving g-C_3N_4 photocatalytic performance[10]. Compared with traditional methods, the penetration of the precursor solution into the pore structure of the template will induce the synthesis of g-C_3N_4 with different morphologies. The filling of the precursor solution in the template hole channel directly affects the final morphology of the carbon nitride product.

There are three main steps to prepare g-C_3N_4 by hard-templating method: (1) Immerse the precursor into the template. (2) Dry and roast at high temperature to make the precursor in the pores of the template polycondensate to form g-C_3N_4. (3) The template is removed by using HF or NH_4HF_2 solvent to obtain g-C_3N_4 materials with a mesoporous structure[11-12].

Goettmann[13]prepared mesoporous g-C_3N_4 by hard-templating method. Using mesoporous SiO_2 spheres with a controllable nanostructure as a hard template, the cyanamide precursor was uniformly dispersed in the mesopores of the SiO_2 spheres, and then thermally polymerized. The template was removed with NH_4HF_2 solvent to

obtain mesoporous g-C_3N_4 material with a specific surface area of 86~440 $m^2 \cdot g^{-1}$. Liu et al. [14] used mesoporous SiO_2 nanorods as a template, added the cyanamide precursor to the SiO_2 nanorod pores by dipping, and after high-temperature roasting, to prepare carbon nitride nanorods (CNR) with uniform size distribution. The diameter was about 80 nm, the length was about 200 nm. Song[15] used anodic aluminum oxide (AAO) as a template and ethylenediamine and carbon tetrachloride as precursors. After calcination at 600 ℃ under N_2 atmosphere for 5 h, the AAO template was removed with 2 $mol \cdot L^{-1}$ NaOH solvent to obtain carbon nitride nanotubes with relatively uniform diameter and length.

In summary, the preparation of mesoporous g-C_3N_4 by hard-templating method mainly involves precursor infusion (precursor is uniformly infused in the pores of the hard template), high-temperature polymerization (fired in an inert atmosphere (such as N_2) at high temperature to form a template co-existing product) and template removal in these three steps. However, due to the reaction of HF or NH_4HF_2 solution with g-C_3N_4 during the removal process, the actually obtained g-C_3N_4 product has a large amount of uncondensed -NH_2, -NH-, -N- and other N-containing functional groups at the edge of the graphite layer. This is determined by the inherent properties of hard-templating method to prepare mesoporous g-C_3N_4 by using HF or NH_4HF_2 solution to remove the template.

4.2 Soft-templating method

The soft-templating method refers to a preparation method in which surfactants, ionic liquids or bubbles are used as soft templates to obtain mesoporous g-C_3N_4 after high temperature polymerization and carbonization with a nitrogen-containing precursor. For example: Surfactant molecules can spontaneously form structurally ordered supramolecular structures under certain conditions. Organic molecules containing N precursors can interact with surfactant molecules (mainly including hydrogen bonds, electrostatic forces, van der Waals forces) self-assembly on the surface of supramolecular, and then the template molecule is removed by high temperature calcination to form the mesoporous g-C_3N_4[16]. Wang[17] used non-ionic

surfactants (such as P123) as structure-directing agents for the synthesis of g-C_3N_4. They first mixed the precursor dimeric cyanamide and the soft template to dissolve in water, and after drying and high-temperature roasting to remove the soft template, g-C_3N_4 could be generated. The focus of the preparation process was to use a multi-step temperature programmed roasting method to obtain the required materials. It was worth noting that the pore size distribution of the product obtained by this method is not uniform enough.

Shen[18] used Triton X-100 as a template, melamine and glutaraldehyde as precursors, and prepared g-C_3N_4 with bimodal pore diameters after condensation and carbonization. The mesopore pore diameters were concentrated at 3.8 and 10-40 nm, respectively. After analysis, mesopores with smaller pore diameters were formed by removing the template. Yan[19] used Pluronic P123 and melamine molecules as soft templates and precursors, respectively. Melamine self-assembled on the surface of Pluronic P123, dried and calcined to prepare mesoporous g-C_3N_4. The results of elemental analysis experiments showed that when the P123 template was not added, the molar ratio of C to N of g-C_3N_4 was 0.65; with the gradual increase in the amount of P123 added, the molar ratio of C to N rose from 0.65 to 0.69. Shen[20] synthesized polystyrene by emulsion polymerization and used this as a soft template to prepare porous g-C_3N_4. During this process, they mainly studied the influence of the template on the chemical composition, crystal structure and surface structure of the product. The experimental results showed that the specific surface area and porosity of g-C_3N_4 can be controlled by adjusting the amount of polystyrene. Elemental analysis experiments further showed that the atomic ratio of C and N in the resulting product increase with the increasing of polystyrene, but it was lower than the theoretical value, which was consistent with Yan's research results. This was caused by residual amino groups caused by incomplete polycondensation, in which the residual N atoms mainly exist in the form of -NH_2, -NH- at the edges of the graphite layer network structure.

The bubble soft template is generally formed by volatilization or decomposition and gasification of NH_4Cl, sulfur and sucrose at high temperature. Iqbal[21] used melamine as the precursor and NH_4Cl as the soft template to synthesize mesoporous

g-C_3N_4. By adjusting the mass ratio of melamine/NH_4Cl, the specific surface area of the prepared g-C_3N_4 material ranged from 17 to 195 $m^2 \cdot g^{-1}$. In addition, He[22] used melamine as a precursor and sublimed sulfur as a soft template to synthesize porous g-C_3N_4. They first uniformly mixed sublimed sulfur and melamine, and melted the sublimated sulfur to promote the diffusion and contact of precursor molecules during heating. At high temperature, melamine thermally polycondensated and rearranged to form tri-s-triazine. As the temperature rose further, the sulfur volatilized into bubbles and be used as a template (the pore structure was created around the bubbles during the polymerization process). Finally, after the sulfur bubbles are removed, the tri-s-triazine structural unit was polycondensed to form porous g-C_3N_4 with a specific surface area of up to 46 $m^2 \cdot g^{-1}$.

4.3 No-templating method

In addition to the soft-templating and hard-templating method, the researchers tried to use the no-templating method to directly heat and synthesize g-C_3N_4. For example: Min[23] prepared mesoporous g-C_3N_4 by using the characteristic of urea thermal decomposition to produce a large amount of small molecule gas. The specific surface area and pore volume of the product were about 51.6 $m^2 \cdot g^{-1}$ and 0.26 $cm^3 \cdot g^{-1}$, respectively. Han[24] put 2 g of dimeric cyanamide in a ship-shaped crucible, covered with another ship-shaped crucible, forming a semi-closed system, and then placed the semi-closed system in the muffle furnace at 2.2 ℃·min^{-1}. The heating rate was increase to 550 ℃ and kept for 4 h, so that the specific surface area and pore volume of mesoporous g-C_3N_4 material were 201~209 $m^2 \cdot g^{-1}$ and 0.50~0.52 $cm^3 \cdot g^{-1}$. Kumar[25] put the product obtained by direct roasting of melamine in an ethanol-water mixed solution, and sonicated it at room temperature with 33 Hz ultrasound for 5 h. After subsequent separation and drying, the mesoporous graphite phase carbon nitride can be obtained. In addition, carbon nitride can also be obtained through supramolecular self-assembly and thermal condensation process through firing. Tong[26] first hydrothermally heat treated cyanuric acid and melamine to generate hexagonal prism crystals, and then fired the mixture of cyanuric acid-melamine crystals and urea to

form a tubular carbon nitride homotype heterojunction. Guo[27] mixed melamine and phosphorous acid for hydrothermal reaction, and melamine was hydrolyzed to produce cyanuric acid with the aid of phosphorous acid. Cyanuric acid can form hexagonal columnar supramolecules through molecular self-assembly with melamine. This supramolecule was pyrolyzed to obtain a hexagonal tubular structure phosphorus-doped carbon nitride material. The above-mentioned supramolecular self-assembly method did not require template molecules, which had the advantages of simple operation, low cost, and short synthesis period. Furthermore, by reasonably controlling the reaction conditions of the self-assembly process, the composition, morphology and properties of the product can be further effectively controlled[28]. Although the no-templating method has a short preparation cycle, its repeatability is lower than that of the hard template method. Besides, the specific surface area of the product is lower. Similar to the soft-templating method, the no-templating method also requires strict control of the preparation conditions, and the texture properties and N content of the product cannot be accurate prediction.

In summary, the three preparation methods in the thermal polymerization method have their own advantages and disadvantages (**Table 1**), so they need to be comprehensively considered in the synthesis process based on the actual use of the material.

Table 1. Advantages and disadvantages of g-C_3N_4 preparation methods

Methods	Advantages	Disadvantages
Hard-templating	1) adjustable pore structure	1) expensive hard template
	2) products with more ordered mesopores and high specific surface area	2) affect the N content
		3) corrosive and harmful to the environment
Soft-templating	1) simple and low-cost	1) wide pore size distribution
	2) environmental friendly	2) low product yield
Non-templating	no template required	1) disordered pores and

		wide pore size distribution
		2) low repeatability

5 Modification of g-C_3N_4 photocatalytic material in CO_2 reduction

In addition to the selection of the preparation method mentioned in the previous chapter, the performance of the g-C_3N_4 catalyst can also be optimized through various approaches such as doping and compounding.

The photocatalytic reaction of g-C_3N_4 includes three steps, (1) photogeneration of carriers excited by visible light, (2) transfer of carriers to the catalyst surface, and (3) electrons and holes to initiate chemical reactions. In addition, due to the Coulomb force, light-induced charges may recombine. In order to obtain excellent photocatalytic activity, the photocatalyst should have a wide range of photo-response, fast carrier transfer rate and high redox capability.

So far, researchers have tried many methods to optimize the photocatalytic activity of g-C_3N_4, such as doping elements, functional group modification and construction of heterojunctions. It is important that these modification strategies and the surface behavior of g-C_3N_4 play a major role in the effective photocatalytic performance. On the one hand, all oxidation or reduction reactions related to the photocatalytic process occur on the surface of the photocatalyst. On the other hand, the surface behavior of the photocatalyst will affect the separation and migration of charge carriers. In addition, some special surface modification, such as element doping, surface defect engineering and functional group grafting, can also optimize the band structure of g-C_3N_4, thereby greatly improving its light utilization efficiency.

Therefore, we will summarize the different modification methods and describe the effect of different modification methods on g-C_3N_4 in improving photocatalytic CO_2 reduction.

5.1 Surface engineering

Reasonable development and design of new surface strategies is a promising approach because it has significant advantages in separating photo-generated charges and improving sunlight utilization. Therefore, on the g-C_3N_4 based photocatalytic

material, through surface engineering modification, CO_2 reduction can be realized more efficiently.

Surface engineering can improve the photocatalytic performance of g-C_3N_4 by adjusting and optimizing its basic structural units. It mainly involves functional group modification, surface defect modification.

5.1.1 Functional group modification

Adjusting the molecular structure of g-C_3N_4 to extend its light response and reduce light-induced charge recombination is an effective way to enhance the photocatalytic performance of g-C_3N_4[29-31]. Taking into account the organic properties of the g-C_3N_4 conjugated structure, it is very feasible to adjust the molecular composition through copolymerization to prepare the g-C_3N_4. It is worth noting that the diversity of organic reactions can use N-rich precursors and comonomers to modify g-C_3N_4, thereby providing a variety of methods for designing supramolecules. The surface properties, texture and electronic structure of g-C_3N_4 can be optimized by introducing special functional groups into the g-C_3N_4 conjugated system by means of copolymerization[32].

Grafting aromatic compounds into the melon network will change the electronic distribution of the g-C_3N_4 system, thereby optimizing its inherent electronic/optical properties[33-34]. For example, Shi et al. reported a general and effective Schiff base chemical method for the construction of aromatic grafted g-C_3N_4-based copolymers. According to this method, various aromatic hydrocarbons can be grafted into melon units. All the prepared g-C_3N_4 showed excellent photocatalytic hydrogen production performance under visible light. In addition, the co-monomer used in this study has low cost and small addition.

In addition to grafting aromatic compounds into the carbon nitride network, thioacetamide was used as a co-monomer of urea to prepare sulfur-doped end-methylated g-C_3N_4 nanosheets (SMCN) (As shown in **Fig 3**). Density functional theory (DFT) showed that doping S atoms into the methyl-modified melon network can induce VB near the Fermi level to form a special intermediate energy gap state,

thereby greatly reducing the energy gap (~0.7 eV) [35].

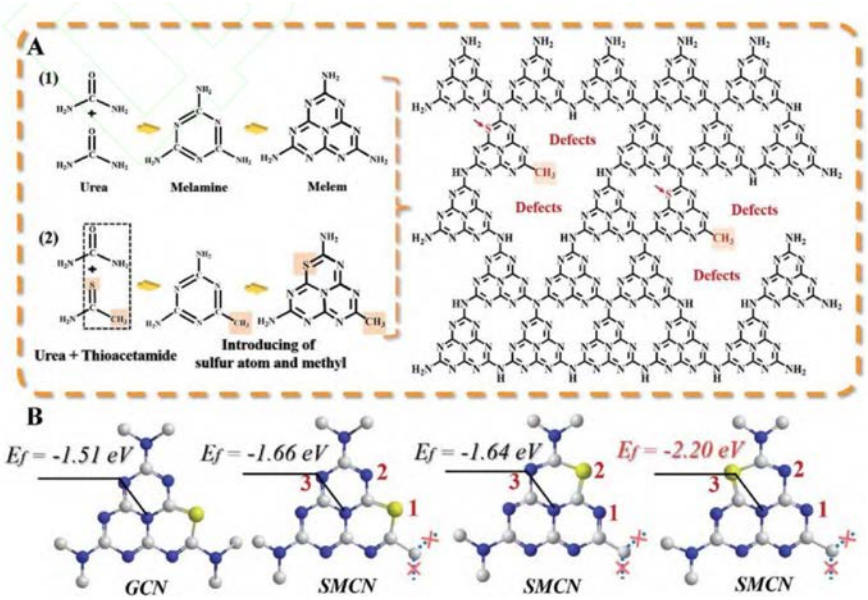

Fig. 3. (A) Illustration for fabrication of the S doping methyl-modified g-C_3N_4. (B) The formation energy (E_f) of substitute possible N atoms by S atoms in g-C_3N_4 networks.

5.1.2 Surface defects modification

Defect engineering is an interesting strategy to optimize the photocatalytic efficiency of semiconductor materials. As we all know, defect engineering of g-C_3N_4 can effectively enhance charge separation, optimize the energy band structure and extend the light response. Therefore, various surface defects of g-C_3N_4, such as carbon vacancies, nitrogen vacancies, cyanamide defects and structural edge defects, have been extensively studied in recent years to improve the photocatalytic performance of g-C_3N_4 in CO_2 reduction.

Zhang[36] devised a new strategy to prepare g-C_3N_4 with rich porous structure and heterostructure defects doped with sulfur atoms by processing g-C_3N_4 in the presence of CH_3CN and H_2S. In this special gas environment, the original g-C_3N_4 nanosheets are etched to produce nanopores. In addition, due to the incomplete conversion of H_2S, the melon unit is destroyed to form CS bonds, cyano groups and S. The prepared photocatalyst showed excellent energy band structure, extended light absorption and fast carrier transport, which greatly improved the photocatalytic performance of H_2O decomposition.

5.2 Semiconductor compound

Semiconductor recombination refers to the usage of semiconductor materials with different energy levels and matching relative energy band positions to recombine on the surface of g-C_3N_4. g-C_3N_4 mainly plays two roles. The first is to provide electrons for the system, because g-C_3N_4 has a two-dimensional layered structure with many small in-plane repeating units, and the repeating units have a conjugate structure, so g-C_3N_4 has one The large conjugate structure facilitates electron transmission; the second is to cooperate with other semiconductors to form a heterojunction, promoting the separation and transmission of photogenerated carriers, and the photoelectric conversion efficiency.

According to the heterojunction formed by the recombination of carbon nitride and semiconductor, it can be roughly divided into type II heterojunction, type I heterojunction, type III heterojunction, Schottky junction and Z type heterojunction.

5.2.1 Type II heterojunction

For the type II heterojunction, the band edges of the two semiconductors are arranged staggered, causing the conduction band electrons of the high conduction band semiconductor migrate to the conduction band of the low conduction band semiconductor, and the valence band electrons of the high valence band semiconductor to the low valence band semiconductor. The migration of the valence band causes the photogenerated electrons and holes to accumulate in the low conduction band and low valence band, respectively, inhibiting their recombination. Liu[37] synthesized $ZnIn_2S_4$-g-C_3N_4 nano-layered composite by hydrothermal method. The band structure of $ZnIn_2S_4$ (2.34~2.48 eV) and g-C_3N_4 can be matched to form a type II heterojunction, and the interface between the two close contact, effectively transfer and separate photo-generated carriers (as shown in **Fig 4**). The same type of substrate can also be used as a basis to construct a homogeneous g-C_3N_4 type II heterojunction. For example, Dong[38] used dicyandiamide and urea as precursors, and obtained similar substrates through heat treatment to form g-C_3N_4/ g-C_3N_4 metal-free type II heterojunction. Under visible light irradiation, CN-D (with dicyandiamide as the precursor) The conduction band electrons of carbon nitride obtained by the system

migrate to the conduction band of CN-U (carbon nitride obtained by using urea as the precursor system), and the valence band holes of the latter migrate to the valence band of the former (as shown in the **Fig 5**), to achieve effective separation of electrons and holes.

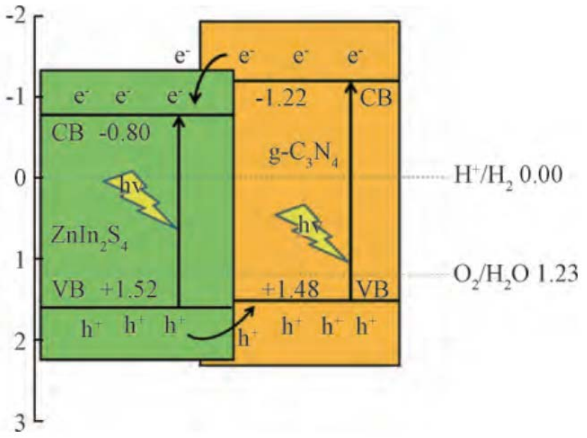

Fig.4. Mechanism for the enhanced photocatalytic activity of $ZnIn_2S_4$-g-C_3N_4 composites

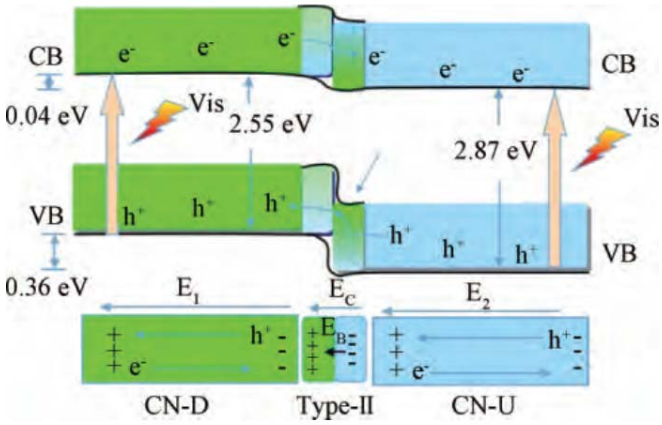

Fig.5. Illustration of photogenerated electrons and holes transfer process on type II g-C_3N_4/ g-C_3N_4 heterostructure under visible light irradiation

5.2.2 Type I and Type III heterojunction

For type I heterojunction, the conduction band and valence band positions of semiconductor 1 are more negative and positive than those of semiconductor 2, respectively, as shown in **Fig 6a**. The electrons and holes generated during light irradiation accumulate in the semiconductor with a narrow band gap through migration. In this case, the electron-hole pairs are not effectively separated, but the photocatalytic activity is reduced.

For type III heterojunction, the conduction band edge and valence band edge of semiconductor 1 are completely higher than the conduction band edge of

semiconductor 2 (**Fig 6b**). The conduction band and valence band edge of the two semiconductors are completely staggered because they are not effective. Ground separation of electron-hole pairs cannot improve their activity, so there are few studies on type I and type III heterojunctions based on g-C_3N_4.

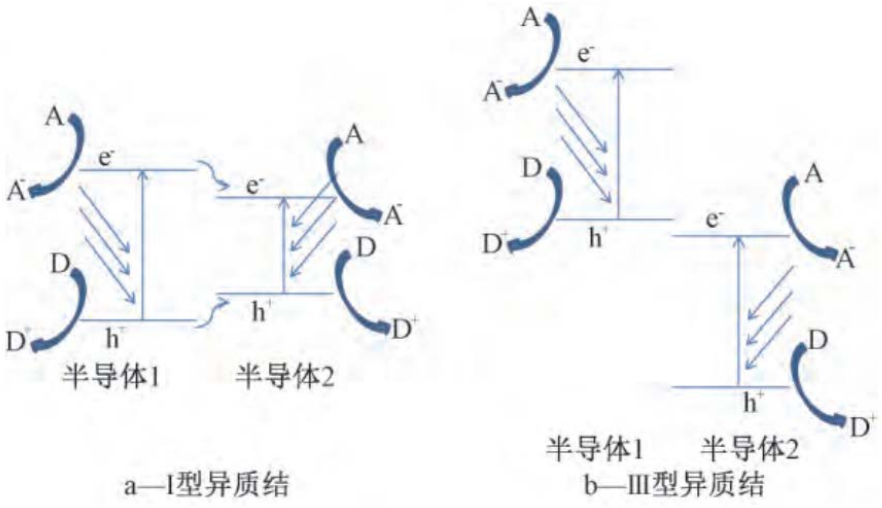

Fig.6. Illustration of photogenerated electrons and holes transferprocess on type I and III heterostructures

5.2.3 Schottky junction

Similar to the TiO_2/Pt system, noble metals such as Pt[39-40], Au[41] and Pd[42] are generally used as promoters to form Schottky junctions with g-C_3N_4. Noble metals have a high work function and can be used as electron traps to capture and store photogenerated electrons. It is effectively separated from the space of the photo-generated holes, improving its hydrogen production activity. There are also studies on using transition metals as co-catalysts to form Schottky junctions with g-C_3N_4 to improve its activity[43-44]. Bi et al. used solvothermal method to use melamine and nickel acetylacetonate as precursors, and loaded Ni on g-C_3N_4 to form Schottky junction. The band bending phenomenon was observed, which can effectively separate photogenerated carriers and greatly improve the yield of H_2. In addition to metals, organic carbon materials, graphene, and carbon nanotubes can act as co-catalysts to accept g-C_3N_4 photogenerated electrons due to their excellent electrical conductivity. Ong[45] prepared 2D/2D rGO/pCN heterojunction catalysts through electrostatic self-assembly, which formed an intimate contact between the

two, which effectively separated carriers at the heterojunction interface and prevented the recombination of electron-hole pairs. , Effectively improve the performance of photocatalytic reduction of CO_2.

5.2.4 Z type heterojunction

The Z-type heterojunction is similar to the type II heterojunction in the energy band structure, but the electron hole flow direction is different, so its redox performance is different. The conduction band electrons of the low conduction band semiconductor combine and annihilate with the valence band holes of the low valence band semiconductor, making the valence band holes of the former and the conduction band electrons of the latter are effectively separated, and the redox effect is exerted. Therefore, this heterojunction not only has a wide spectral absorption range, but also has a high redox capability, which effectively solves the problem of reduced redox properties caused by carrier migration in type II heterojunctions. The most typical is the Z-type heterojunction composed of WO_3 and g-C_3N_4. The band gap of WO_3 is 2.7~2.8 eV, which is close to the band gap of g-C_3N_4, and the conduction band and valence band sides are more positive than g-C_3N_4, which can form staggered band-edge potential energy, satisfying the structure of Z-type heterojunction[46]. The research of Chen[47] showed that when g-C_3N_4 is the main part, it formed a Z-type heterojunction with WO_3, and the valence band holes of g-C_3N_4 quickly recombined with the conduction band electrons of WO_3, resulting in photogenerated electrons of g-C_3N_4 and WO_3. Photo-generated holes accumulate, and its photocatalytic activity for degrading BF was more than doubled compared with g-C_3N_4 and WO_3 (as shown in **Fig 7**).

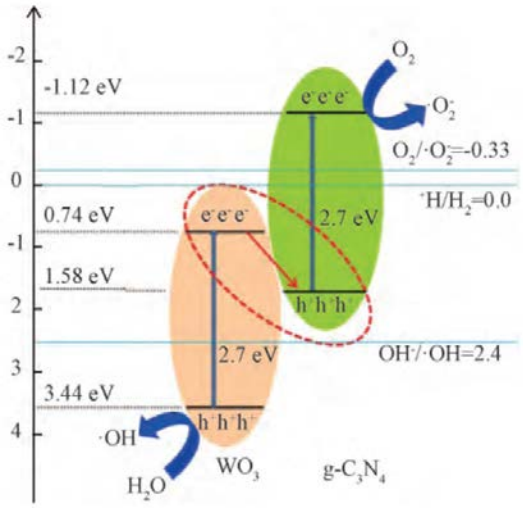

Fig.7. Separation mechanisms of photogenerated electrons andholes on WO_3/g-C_3N_4 heterojunction

5.3 Element doping

Doping usually refers to the purposeful incorporation of a small amount of other elements or compounds into the matrix to change the crystal phase structure, electronic distribution or surface state. It is a commonly used modification method for preparing high-efficiency catalysts.

5.3.1 Non-metallic element doping

The doping of non-metals[48-51], such as B, S, O, P, F, C, etc., can replace the C, N, and H elements in the 3-s-triazine structural unit, resulting in the replacement of lattice defects and effectively suppressing recombination of electron-hole to improve the photocatalytic performance of g-C_3N_4. Zhai et al. applied first principles to study the changes caused by S and O doping quantum g-C_3N_4. It is found that S and O doping can replace N atoms in different positions in g-C_3N_4 and cause changes in the surrounding C-N bonds, significantly reducing the HOMO-LUMO energy gap. The macroscopic improvement of optical performance was manifested in broadening the light response range and increasing the light absorption intensity, and the higher the doping concentration, the more obvious the improvement in optical performance. It can be seen that non-metal doping is of great significance for improving photocatalytic activity, and has important research value in the field of photocatalytic reduction of CO_2.

Li[34] doped g-C_3N_4 with S to investigate the reaction mechanism of reducing CO_2. It is found that the doping of S is easier to replace the N atoms at the edge of g-C_3N_4 and form hybridization with C atoms. Since the atomic radius of S atoms (r=100 pm) is larger than that of N atoms (r=65 pm), the crystal structure changes significantly after doping. Besides, the number of free electrons increases after light excitation, and the Fermi level moves up. It exhibits typical n-type doping. Han et al. used P-doped g-C_3N_4 to prepare BP@ g-C_3N_4 catalyst for photocatalytic reduction of CO_2. After P doping, it was easy to replace the C atoms in g-C_3N_4, which significantly changed the crystal structure of g-C_3N_4 and appears as n-type doping. After the doping, the Fermi energy level has shifted significantly, and a new energy band was generated on the basis of the original energy band structure, which had an important influence on the adjustment of the g-C_3N_4 energy band structure. The reduction rate of CO_2 increased from 2.65 $\mu mol \cdot g^{-1} \cdot h^{-1}$ to 6.54 $\mu mol \cdot g^{-1} \cdot h^{-1}$, which significantly improved the photocatalytic performance.

Taking O and S doped g-C_3N_4 as an example, **Table 2** showed the HOMO-LUMO band gap binding energy of different doping sites. It can be seen from **Table 2** that the HOMO-LUMO energy gap was significantly reduced when the elements are doped, indicating that the doping of O and S can significantly improve the energy level structure and electronic distribution of g-C_3N_4. In addition, different elements doping at the same site and the same element doping at different sites play different roles in the regulation of energy levels. The photocatalytic reduction after O and S doping was shown in **Fig 8**. Different doping sites and different doping elements had different effects on the light absorption properties. Lowering the band gap energy can effectively increase the light absorption range, improve the light absorption and catalytic activity. When CO_2 molecules were adsorbed on the catalyst surface, more energy was used to overcome the energy barrier, so that the reduction yield of CO_2 was improved.

Table 2. The total energy, HOMO-LUMO energy gap, minimum frequency and impurity formation energy of doped structures at different sites of O and S

Structure	Energy/eV	HOMO-LUMO energy	Frequency/cm^{-1}	Formation

		gap		energy/eV
$(g\text{-}C_3N_4)_6$	-793.481	1.863	33.209	
$(g\text{-}C_3N_4)_6$-N2-O	-790.149	0.256	17.174	-0.682
$(g\text{-}C_3N_4)_6$-N3-O	-790.330	0.574	26.571	-0.863
$(g\text{-}C_3N_4)_6$-N8-O	-790.283	0.371	24.827	-0.816
$(g\text{-}C_3N_4)_6$-N2-S	-787.122	0.326	23.748	1.714
$(g\text{-}C_3N_4)_6$-N3-S	-787.433	0.684	24.892	1.403
$(g\text{-}C_3N_4)_6$-N8-S	-787.621	0.617	25.196	1.215

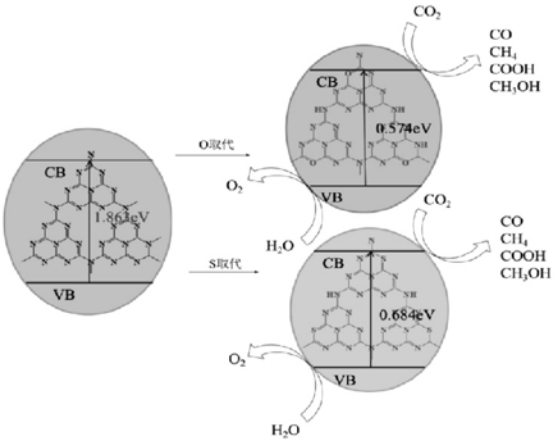

Fig 8. S, O doped $g\text{-}C_3N_4$ photocatalytic reduction of CO_2 reaction mechanism

5.3.2 Metal doping

After the metal doped with $g\text{-}C_3N_4$, electrons are transferred from the metal to the adjacent N or C atoms, changing the electron density of the N or C atoms, and then affecting the electronic structure and energy band position of $g\text{-}C_3N_4$. Metals such as Cu[52], Ag, Au[53], Fe[54], Pt[55-56] can be doped into $g\text{-}C_3N_4$, causing lattice defects. Li[57] found that the doping of Cu and Mo change the electron distribution and energy band structure of $g\text{-}C_3N_4$, and at the same time changed the reaction path on the surface of $g\text{-}C_3N_4$, which promoted the adsorption and activation of CO_2 on the catalyst surface, effectively reducing the activation energy during reduction process.

Beenish[52] used Cu doped with rod-shaped $g\text{-}C_3N_4$ to investigate the performance and product distribution of CO_2 reduction in different reaction systems. It was found that Cu in the form of Cu^{2+} was doped in $g\text{-}C_3N_4$, and significantly affected the energy level structure of $g\text{-}C_3N_4$. In different reaction systems, different main products are

obtained by reduction. In the CO_2-H_2O reaction system, the main product is CH_4, and the reaction rate was 1.84 times that of pure g-C_3N_4, In the CO_2-CH_4 reaction system, the main product For CO and H_2, the reaction rate was 1.33 times that of pure g-C_3N_4. Yu[37] used Pt-doped g-C_3N_4 to reduce CO_2 to prepare hydrocarbons. It is found that Pt exists in g-C_3N_4 in the form of atoms, but after the reduction reaction occurs, part of Pt exists in the form of ions. And the different doping amounts of Pt made the reduction products of CO_2 different selectivity, and the main product of CO_2 reduction by pure g-C_3N_4 was CH_3OH. When the doping amount of Pt is 5%, the main products of reducing CO_2 were CH_4 and HCHO; when the doping amount is 10%, the main products was CH_4.

The reaction mechanism of metal-doped g-C_3N_4 applied to photocatalytic reduction of CO_2 was shown in **Fig 9**. The Fermi level of g-C_3N_4 is close to the bottom of CB. The metal doping makes the Fermi level move, and the dopant orbital hybridizes with the C or N electron orbital to form a new electron orbital, which effectively improve the oxidation-reduction performance of the catalyst and overcome the energy barrier of photocatalytic reduction of CO_2. When the light source is illuminated, the valence band electrons on the catalyst were excited to the conduction band. Then a series of reduction reactions occur on the conduction band, and the holes on the valence band undergo oxidation reactions.

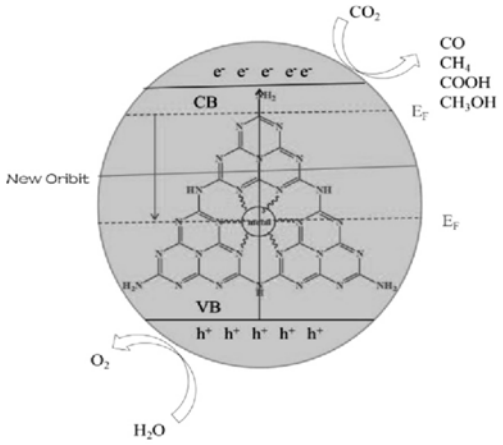

Fig. 9. Metal-doped g-C_3N_4 photocatalytic reduction of CO_2 reaction mechanism

5.4 Specific surface area control modification technology

Usually g-C_3N_4 prepared from N-containing precursors (such as urea, melamine,

dicyandiamine, etc.) through high-temperature polycondensation is shown as bulk particles or lamellar polymers with a small specific surface area (<10 m^2/g), greatly restricting its application. Regardless of the doping modification technology or the semiconductor compound modification, the interaction only occurs on the surface of g-C_3N_4. Therefore, effectively regulating the g-C_3N_4 nanostructure and expanding its specific surface area not only makes the performance of g-C_3N_4 more stable, but also increases reactive sites, which is an effective way to improve the photocatalytic activity of g-C_3N_4.

5.4.1 Mesoporous g-C_3N_4

The introduction of nano-scale porous structure into the bulk g-C_3N_4 can significantly increase the specific surface area of g-C_3N_4, which is beneficial to increase the reaction contact area and reactive sites, thereby improving its catalytic performance. Using ordered silicon-based materials as hard templates, porous carbon nitride materials with adjustable pore structure and pore size can be synthesized. It was reported that Zhao et al. use SBA-15 and a new type of cross-linked bimodal mesoporous SBA-15 (CLBM-SBA-15) as a hard template to prepare mesoporous g-C_3N_4. The resulting g-C_3N_4 (CLBM- SBA-15) had a morphology similar to mesoporous SiO_2, and numerous pores are formed on the surface of g-C_3N_4. In the photocatalytic degradation test of methyl orange, the activity of mesoporous g-C_3N_4 was nearly 15.3 times that of bulk g-C_3N_4 (the results were shown in **Fig 7**). Such high photocatalytic performance was due to the fact that the mesoporous g-C_3N_4 has high specific surface area, pore volume and active reaction sites. Shi et al. synthesized mpg-CN in situ using TEOS as a mesoporous template and cyanamide as a precursor, and the specific surface area of mpg-CN reached 152 m^2/g. Its photocatalytic effect on the degradation of RhB was remarkable. This can be attributed to the high specific surface area and high electron-hole pair separation efficiency of mpg-CN, which enhanced the dye adsorption capacity of mpg-CN. And mpg-CN still performed well after being recycled for 3 times. The in-situ synthesis method provided a simple preparation method for the mesoporous graphite carbon photocatalyst.

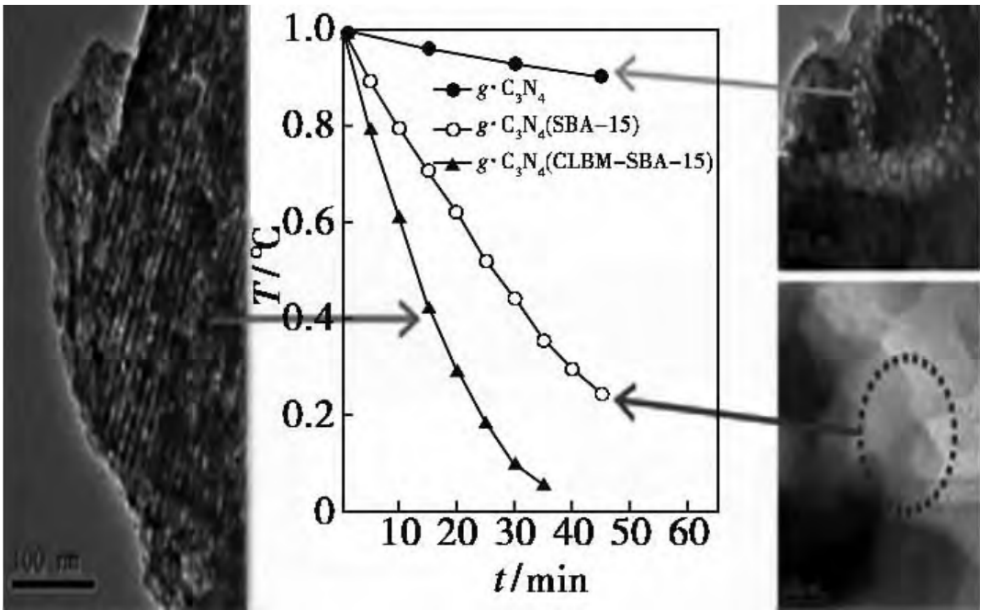

Fig. 10. The sample degraded methyl orange under visible light irradiation

Song[58] prepared the mesoporous high specific surface area g-C_3N_4 by the hard template method for photocatalytic reduction of CO_2 and hydrolysis of hydrogen. The yields of H_2, CO, and C_2H_5OH were 2.3, 0.7, 4.0 μmol·g^{-1}·h^{-1}, which were 1.36, 7, and 1.74 times of lump g-C_3N_4, respectively, and the selective reduction increased from 46.5% to 57.4%.

In addition, Dong[59] used melamine hydrochloride instead of melamine, and directly calcined at high temperature to synthesize g-C_3N_4 with a porous structure (as shown in **Fig 11a**), without a template, and the reaction was simple and controllable. The specific surface area of porous g-C_3N_4 is increased by 39 times, and the optical band gap was increased by 0.13 eV. Adding thiourea or increasing the heating rate of calcination will result in a larger specific surface area and a better porous structure, resulting in better adsorption and photodegradation activity[60].

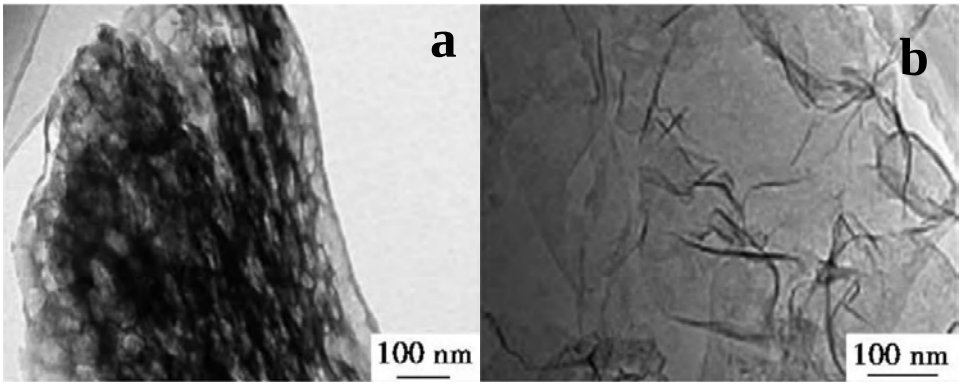

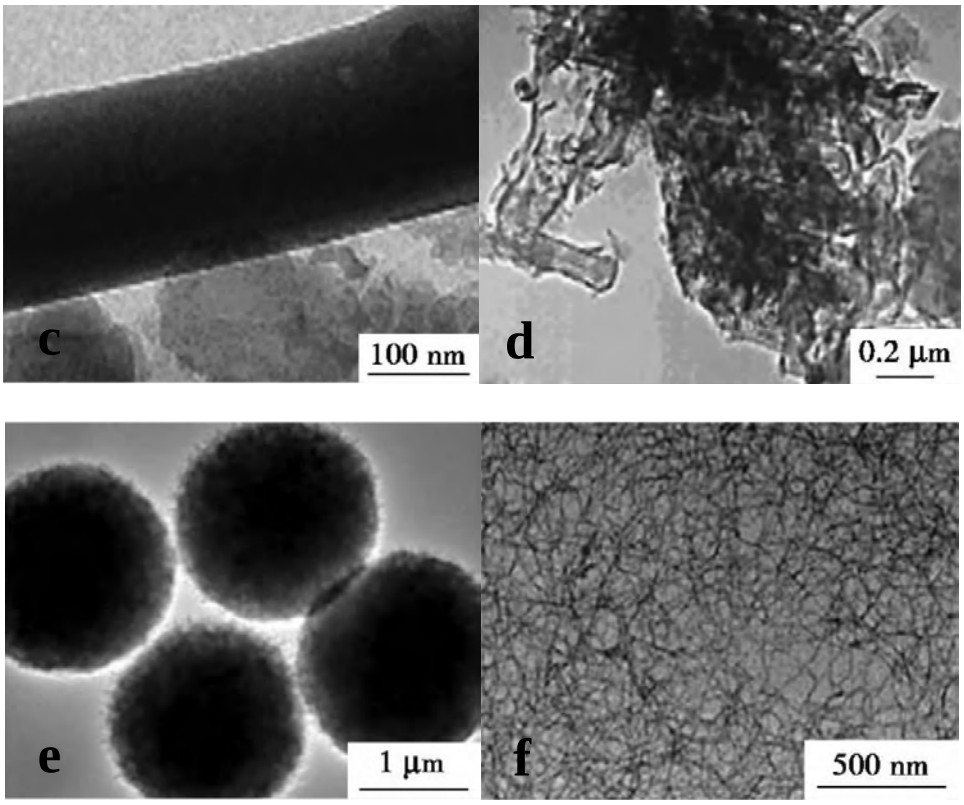

Fig. 11. g-C_3N_4 with different microstructures: (a) porous g-C_3N_4; (b) nano-thin layer; (c) nanorod; (d) nanotube; (e) nanosphere; (f) nanofiber

5.4.2 Nanoflakes

The bulk g-C_3N_4 was prepared into a nano-thin layer or even a single-layer structure by means of exfoliation. The process was similar to that of exfoliating graphite to prepare graphene. Due to its unique structure and properties, related research has gradually received attention in recent years and developed rapidly.

The methods commonly used to prepare g-C_3N_4 nano-thin layers mainly include solvent stripping and thermal stripping. Solvent stripping refers to the stripping in water, methanol, isopropanol and other solvents. For example, Yang[61] performed liquid phase stripping of the bulk g-C_3N_4 in isopropanol, and the thickness of the prepared g-C_3N_4 nano-thin layer was only 2 nm. The thermal stripping method was the thermal oxidation and corrosion treatment of g-C_3N_4 in air, so that the block g-C_3N_4 was gradually separated into nano-scale nano-thin layers[62]. Because the thin layer of g-C_3N_4 had a thinner thickness, larger specific surface area and improved electron transfer ability, it was beneficial to separate photo-generated electron-hole pairs, effectively prolong the life of photo-generated carriers, which used in

photo-splitting water to produce hydrogen exhibiting excellent catalytic activity.

The ideally peeled g-C_3N_4 is a single layer or several layers, connected by carbon and nitrogen covalent bonds, having high mechanical strength and good electrical properties. This should be the direction of future research efforts on g-C_3N_4 nano-thin layers. If successfully, it will be another peak in the research and application of carbon nitride materials.

5.4.3 g-C_3N_4 with different morphologies

The nano-scale g-C_3N_4 has different morphologies, but all of them can expand the specific surface area, which is conducive to better contact between the reactant and the catalyst in practical applications. It also reduces the time for electron-hole pairs to transfer from the interior of the bulk to the surface, so that the recombination rate of electron-hole pairs is reduced, thereby improving catalytic activity. By controlling the preparation process to nano-size g-C_3N_4, nanorods[63], nanotubes[64], nanospheres[65], and nanofibers[66] with different morphologies can be prepared (as shown in **Fig 11c-11f**).

After refluxing g-C_3N_4 with methanol, Zhu[63] realized the conversion of g-C_3N_4 from nano-sheet-like to nano-rod-like structure. He believed that the possible formation mechanism of g-C_3N_4 nanorods is that g-C_3N_4 nanosheets are first peeled off in methanol solution, and then curled to grow. The reflow process eliminates surface defects and increases the active lattice area, thereby enhancing the photocatalytic activity and photocurrent response intensity. Its photocatalytic activity and photocurrent response intensity were increased by 1.5 times and 2.0 times, respectively. Zeng[64] first obtained g-C_3N_4 nanosheets by ultrasonic liquid phase exfoliation of bulk carbon nitride, then heated the dried g-C_3N_4 nanosheets in a high temperature environment of 350 ℃ for 10 minutes and then quickly transferred to cold water. Because the hot-cold alternately generated thermal stress, the g-C_3N_4 nanosheets gradually curls to obtain carbon nitride nanotubes (C_3N_4 NTs). The entire evolution process was shown in **Fig 11**. The photo-generated carrier had high transmission efficiency and excellent mass transfer ability.

By adjusting the nanostructure of g-C_3N_4, g-C_3N_4 with different morphology and particle size can be obtained. However, the micro-morphology formation, catalytic mechanism, selectivity and other issues have not yet been uniformly and completely answered, and follow-up is still needed the study.

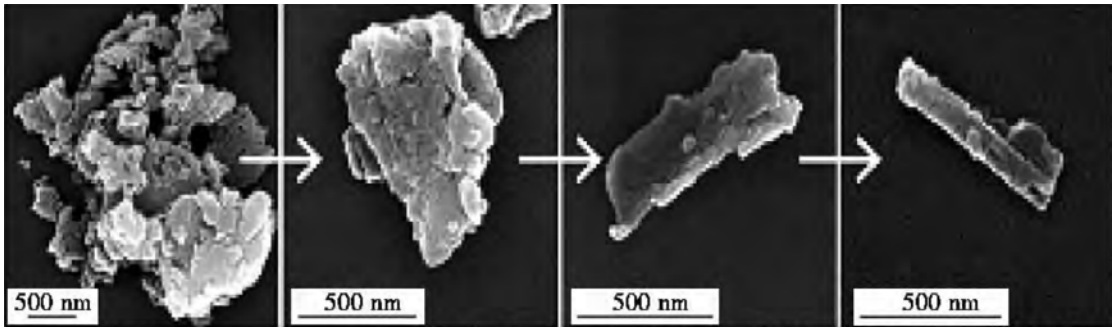

Fig. 12. FESEM of the morphology evolution of C_3N_4 NTs (a) bulk C_3N_4; (b) g- C_3N_4 nanosheets after peeling; (c) half-rolled C_3N_4 NTs; (d) fully rolled C_3N_4 NTs

6 Conclusions

g-C_3N_4 is a non-metallic green catalyst, but it is difficult to reduce CO_2 due to the limitations of g-C_3N_4 itself. By increasing the specific surface area of g-C_3N_4, doping with metal/non-metal, forming heterojunction with p-type semiconductor, etc. Ways to improve the shortcomings of poor conductivity, adjust the energy level structure to improve the redox performance. The high activation energy and low selectivity required in the reaction have always been barriers to industrial applications. With the continuous development of theoretical calculations and experimental research, the continued development of g-C_3N_4-based catalysts has important research significance in the field of photocatalysis.

Bibliography

1. Chang, X.; Wang, T.; Gong, J., CO2 photo-reduction: insights into CO2 activation and reaction on surfaces of photocatalysts. *Energ. Environ. Sci.* **2016,** *9* (7), 2177-2196.
2. Xiang, Q.; Cheng, B.; Yu, J., Graphene-Based Photocatalysts for Solar-Fuel Generation. *Angew. Chem. Int. Ed. Engl.* **2015,** *54* (39), 11350-66.
3. Tu, W.; Zhou, Y.; Liu, Q.; Yan, S.; Bao, S.; Wang, X.; Xiao, M.; Zou, Z., An In Situ Simultaneous Reduction-Hydrolysis Technique for Fabrication of TiO2-Graphene 2D Sandwich-Like Hybrid Nanosheets: Graphene-Promoted Selectivity of Photocatalytic-Driven Hydrogenation and Coupling of CO2into Methane and Ethane. *Adv. Funct. Mater.* **2013,** *23* (14), 1743-1749.
4. Li, J.; Gao, X.; Zhu, L.; Ghazzal, M. N.; Zhang, J.; Tung, C.-H.; Wu, L.-Z., Graphdiyne for crucial gas involved catalytic reactions in energy conversion applications. *Energ. Environ. Sci.* **2020,** *13* (5), 1326-1346.
5. Zuo, Z.; Li, Y., Emerging Electrochemical Energy Applications of Graphdiyne. *Joule* **2019,** *3* (4), 899-903.
6. Zhou, J.; Li, J.; Liu, Z.; Zhang, J., Exploring Approaches for the Synthesis of Few-Layered Graphdiyne. *Adv Mater* **2019,** *31* (42), e1803758.
7. Graphdiyne: A New Photocatalytic CO2 Reduction Cocatalyst. *Adv. Funct. Mater.* **2019**, 1904256.
8. Shen, M.; Zhang, L.; Shi, J., Converting CO2 into fuels by graphitic carbon nitride-based photocatalysts. *Nanotechnology* **2018,** *29* (41), 412001.
9. Savateev, A.; Chen, Z. P.; Dontsova, D., Baking 'crumbly' carbon nitrides with improved photocatalytic properties using ammonium chloride. *RSC Adv.* **2016,** *6* (4), 2910-2913.
10. Huang, J.; Ho, W.; Wang, X., Metal-free disinfection effects induced by graphitic carbon nitride polymers under visible light illumination. *Chem. Commun.* **2014,** *50* (33), 4338-4340.
11. Li, M.; Zhang, S.; Liu, X.; Wang, H.; Han, J., Polymeric Semiconductor Carbon Nitride Prepared from Hard Template. *Journal of Chemical Engineering of Chinese Universities* **2017,** *31* (4), 749-762.
12. Liu, L.; Zhang, W.; Wang, Y., Graphitic carbon nitride materials: controllable preparations and applications in energy catalysis. *CIESC Journal* **2018,** *69* (11), 4577-4591.
13. Goettmann, F.; Fischer, A.; Antonietti, M.; Thomas, A., Chemical synthesis of mesoporous carbon nitrides using hard templates and their use as a metal-free catalyst for Friedel-Crafts reaction of benzene. *Angew. Chem. Int. Ed. Engl.* **2006,** *45* (27), 4467-71.
14. Liu, J.; Huang, J.; Zhou, H.; Antonietti, M., Uniform graphitic carbon nitride nanorod for efficient photocatalytic hydrogen evolution and sustained photoenzymatic catalysis. *ACS Appl Mater Interfaces* **2014,** *6* (11), 8434-40.
15. Bian, S. W.; Ma, Z.; Song, W. G., Preparation and Characterization of Carbon Nitride Nanotubes and Their Applications as Catalyst Supporter. *J.phys.chem.c* **2009,** *113* (20), 8668-8672.
16. Wang, Y.; Jiang, Q.; Shang, J. K.; Xu, J.; Li, Y. X., Advances in the Synthesis of Mesoporous Carbon Nitride Materials. *Acta Physico-Chimica Sinica* **2016,** *32* (8), 1913-1928.
17. Wang, Y.; Wang, X. C.; Antonietti, M.; Zhang, Y. J., Facile One-Pot Synthesis of Nanoporous Carbon Nitride Solids by Using Soft Templates. *Chemsuschem* **2010,** *3* (4), 435-439.
18. Shen, W.; Ren, L.; Zhou, H.; Zhang, S.; Fan, W., Facile one-pot synthesis of bimodal mesoporous carbon nitride and its function as a lipase immobilization support. *J. Mater. Chem.* **2011,** *21* (11), 3890.
19. Yan, H. J., Soft-templating synthesis of mesoporous graphitic carbon nitride with enhanced photocatalytic H-2 evolution under visible light. *Chem. Commun.* **2012,** *48* (28), 3430-3432.

20. Shen, T.; Zhang, J.; Jiang, L.; Dan, Y., Synthesis of porous graphitic carbon nitride by using polystyrene soft templates. *Chemical Research and Application* **2017,** *29* (6), 873-877.
21. Iqbal, W.; Dong, C. Y.; Xing, M. Y.; Tan, X. J.; Zhang, J. L., Eco-friendly one-pot synthesis of well-adorned mesoporous g-C3N4 with efficiently enhanced visible light photocatalytic activity. *Catal. Sci. Technol.* **2017,** *7* (8), 1726-1734.
22. He, F.; Chen, G.; Yu, Y. G.; Zhou, Y. S.; Zheng, Y.; Hao, S., The sulfur-bubble template-mediated synthesis of uniform porous g-C3N4 with superior photocatalytic performance. *Chem. Commun.* **2015,** *51* (2), 425-427.
23. Min, S. X.; Lu, G. X., Enhanced Electron Transfer from the Excited Eosin Y to mpg-C3N4 for Highly Efficient Hydrogen Evolution under 550 nm Irradiation. *J. Phys. Chem. C* **2012,** *116* (37), 19644-19652.
24. Han, K. K.; Wang, C. C.; Li, Y. Y.; Wan, M. M.; Wang, Y.; Zhu, J. H., Facile template-free synthesis of porous g-C3N4 with high photocatalytic performance under visible light. *RSC Adv.* **2013,** *3* (24), 9465-9469.
25. Kumar, S.; Surendar, T.; Kumar, B.; Baruah, A.; Shanker, V., Synthesis of highly efficient and recyclable visible-light responsive mesoporous g-C3N4 photocatalyst via facile template-free sonochemical route. *RSC Adv.* **2014,** *4* (16), 8132-8137.
26. Tong, Z.; Yang, D.; Sun, Y.; Nan, Y.; Jiang, Z., Tubular g-C3N4 Isotype Heterojunction: Enhanced Visible-Light Photocatalytic Activity through Cooperative Manipulation of Oriented Electron and Hole Transfer. *Small* **2016,** *12* (30), 4093-4101.
27. Guo, S.; Deng, Z.; Li, M.; Jiang, B.; Tian, C.; Pan, Q.; Fu, H., Phosphorus-Doped Carbon Nitride Tubes with a Layered Micro-nanostructure for Enhanced Visible-Light Photocatalytic Hydrogen Evolution. *Angewandte Chemie-International Edition* **2016,** *55* (5), 1830-1834.
28. Zheng, Y.; Wang, X., Synthesis of Polymeric Carbon Nitride Photocatalysts by Supramolecular Self-Assembly. *Materials China* **2017,** *36* (1), 25-32.
29. Tian, J.; Zhang, L.; Fan, X.; Zhou, Y.; Wang, M.; Cheng, R.; Li, M.; Kan, X.; Jin, X.; Liu, Z.; Gao, Y.; Shi, J., A post-grafting strategy to modify g-C3N4 with aromatic heterocycles for enhanced photocatalytic activity. *J. Mater. Chem. A* **2016,** *4* (36), 13814-13821.
30. Yang, H.; Zhou, Y.; Wang, Y.; Hu, S.; Wang, B.; Liao, Q.; Li, H.; Bao, J.; Ge, G.; Jia, S., Three-dimensional flower-like phosphorus-doped g-C3N4 with a high surface area for visible-light photocatalytic hydrogen evolution. *J. Mater. Chem. A* **2018,** *6* (34), 16485-16494.
31. Zhang, M.; Duan, Y.; Jia, H.; Wang, F.; Wang, L.; Su, Z.; Wang, C., Defective graphitic carbon nitride synthesized by controllable co-polymerization with enhanced visible light photocatalytic hydrogen evolution. *Catal. Sci. Technol.* **2017,** *7* (2), 452-458.
32. Xu, C.-Q.; Zhang, W.-D., Facile synthesis of nitrogen deficient g-C3N4 by copolymerization of urea and formamide for efficient photocatalytic hydrogen evolution. *Mol. Catal.* **2018,** *453*, 85-92.
33. Zhang, Y.; Wu, L.; Zhao, X.; Zhao, Y.; Tan, H.; Zhao, X.; Ma, Y.; Zhao, Z.; Song, S.; Wang, Y.; Li, Y., Leaf-Mosaic-Inspired Vine-Like Graphitic Carbon Nitride Showing High Light Absorption and Efficient Photocatalytic Hydrogen Evolution. *Advanced Energy Materials* **2018,** *8* (25).
34. Zhou, C.; Zeng, Z.; Zeng, G.; Huang, D.; Xiao, R.; Cheng, M.; Zhang, C.; Xiong, W.; Lai, C.; Yang, Y.; Wang, W.; Yi, H.; Li, B., Visible-light-driven photocatalytic degradation of sulfamethazine by surface engineering of carbon nitride : Properties, degradation pathway and mechanisms. *J. Hazard. Mater.* **2019,** *380*.
35. Li, Y.; Wang, S.; Chang, W.; Zhang, L.; Wu, Z.; Song, S.; Xing, Y., Preparation and enhanced

photocatalytic performance of sulfur doped terminal-methylated g-C3N4 nanosheets with extended visible-light response. *J. Mater. Chem. A* **2019,** *7* (36), 20640-20648.

36. Zhang, X.; Yang, C.; Xue, Z.; Zhang, C.; Qin, J.; Liu, R., Spatial Separation of Charge Carriers via Heterogeneous Structural Defects in Graphitic Carbon Nitride for Photocatalytic Hydrogen Evolution. *Acs Applied Nano Materials* **2020,** *3* (5), 4428-4436.

37. Liu, H.; Jin, Z.; Xu, Z.; Zhang, Z.; Ao, D., Fabrication of ZnIn2S4-g-C3N4 sheet-on-sheet nanocomposites for efficient visible-light photocatalytic H-2-evolution and degradation of organic pollutants. *RSC Adv.* **2015,** *5* (119), 97951-97961.

38. Dong, F.; Ni, Z.; Li, P.; Wu, Z., A general method for type I and type II g-C3N4/g-C3N4 metal-free isotype heterostructures with enhanced visible light photocatalysis. *New J. Chem.* **2015,** *39* (6), 4737-4744.

39. Shiraishi, Y.; Kofuji, Y.; Kanazawa, S.; Sakamoto, H.; Ichikawa, S.; Tanaka, S.; Hirai, T., Platinum nanoparticles strongly associated with graphitic carbon nitride as efficient co-catalysts for photocatalytic hydrogen evolution under visible light. *Chem. Commun.* **2014,** *50* (96), 15255-15258.

40. Li, K.; Zeng, Z.; Yana, L.; Luo, S.; Luo, X.; Huo, M.; Guo, Y., Fabrication of platinum-deposited carbon nitride nanotubes by a one-step solvothermal treatment strategy and their efficient visible-light photocatalytic activity. *Applied Catalysis B-Environmental* **2015,** *165*, 428-437.

41. Bhowmik, T.; Kundu, M. K.; Barman, S., Ultra small gold nanoparticles-graphitic carbon nitride composite: an efficient catalyst for ultrafast reduction of 4-nitrophenol and removal of organic dyes from water. *RSC Adv.* **2015,** *5* (48), 38760-38773.

42. Chang, C.; Fu, Y.; Hu, M.; Wang, C.; Shan, G.; Zhu, L., Photodegradation of bisphenol A by highly stable palladium-doped mesoporous graphite carbon nitride (Pd/mpg-C3N4) under simulated solar light irradiation. *Applied Catalysis B-Environmental* **2013,** *142*, 553-560.

43. Bi, L.; Xu, D.; Zhang, L.; Lin, Y.; Wang, D.; Xie, T., Metal Ni-loaded g-C3N4 for enhanced photocatalytic H-2 evolution activity: the change in surface band bending. *PCCP* **2015,** *17* (44), 29899-29905.

44. Lu, Y.; Chu, D.; Zhu, M.; Du, Y.; Yang, P., Exfoliated carbon nitride nanosheets decorated with NiS as an efficient noble-metal-free visible-light-driven photocatalyst for hydrogen evolution. *PCCP* **2015,** *17* (26), 17355-17361.

45. Ong, W.-J.; Tan, L.-L.; Chai, S.-P.; Yong, S.-T.; Mohamed, A. R., Surface charge modification via protonation of graphitic carbon nitride (g-C3N4) for electrostatic self-assembly construction of 2D/2D reduced graphene oxide (rGO)/g-C3N4 nanostructures toward enhanced photocatalytic reduction of carbon dioxide to methane. *Nano Energy* **2015,** *13*, 757-770.

46. Zhao, G.; Huang, X.; Fina, F.; Zhang, G.; Irvine, J. T. S., Facile structure design based on C3N4 for mediator-free Z-scheme water splitting under visible light. *Catal. Sci. Technol.* **2015,** *5* (6), 3416-3422.

47. Chen, S.; Hu, Y.; Meng, S.; Fu, X., Study on the separation mechanisms of photogenerated electrons and holes for composite photocatalysts g-C3N4-WO3. *Applied Catalysis B-Environmental* **2014,** *150*, 564-573.

48. Yan, S. C.; Li, Z. S.; Zou, Z. G., Photodegradation of Rhodamine B and Methyl Orange over Boron-Doped g-C3N4 under Visible Light Irradiation. *Langmuir* **2010,** *26* (6), 3894-3901.

49. Li, W.; Hu, Y.; Rodriguez-Castellon, E.; Bandosz, T. J., Alterations in the surface features of S-doped carbon and g-C3N4 photocatalysts in the presence of CO2 and water upon visible light exposure. *J. Mater. Chem. A* **2017,** *5* (31), 16315-16325.

50. Li, J.; Shen, B.; Hong, Z.; Lin, B.; Gao, B.; Chen, Y., A facile approach to synthesize novel oxygen-doped g-C3N4 with superior visible-light photoreactivity. *Chem. Commun.* **2012,** *48* (98), 12017-12019.

51. Wang, Y.; Di, Y.; Antonietti, M.; Li, H.; Chen, X.; Wang, X., Excellent Visible-Light Photocatalysis of Fluorinated Polymeric Carbon Nitride Solids. *Chem. Mater.* **2010,** *22* (18), 5119-5121.

52. Tahir, B.; Tahir, M.; Amin, N. A. S., Photo-induced CO2 reduction by CH4/H2O to fuels over Cu-modified g-C3N4 nanorods under simulated solar energy. *Appl. Surf. Sci.* **2017,** *419*, 875-885.

53. Li, H.; Gao, Y.; Xiong, Z.; Liao, C.; Shih, K., Enhanced selective photocatalytic reduction of CO2 to CH4 over plasmonic Au modified g-C3N4 photocatalyst under UV-vis light irradiation. *Appl. Surf. Sci.* **2018,** *439*, 552-559.

54. Song, X.; Tao, H.; Chen, L.; Sun, Y., Synthesis of Fe/g-C3N4 composites with improved visible light photocatalytic activity. *Mater. Lett.* **2014,** *116*, 265-267.

55. Yu, J.; Wang, K.; Xiao, W.; Cheng, B., Photocatalytic reduction of CO2 into hydrocarbon solar fuels over g-C3N4-Pt nanocomposite photocatalysts. *PCCP* **2014,** *16* (23), 11492-11501.

56. Gao, G.; Jiao, Y.; Waclawik, E. R.; Du, A., Single Atom (Pd/Pt) Supported on Graphitic Carbon Nitride as an Efficient Photocatalyst for Visible-Light Reduction of Carbon Dioxide. *J. Am. Chem. Soc.* **2016,** *138* (19), 6292-6297.

57. Li, P.; Wang, F.; Wei, S.; Li, X.; Zhou, Y., Mechanistic insights into CO2 reduction on Cu/Mo-loaded two-dimensional g-C3N4(001). *PCCP* **2017,** *19* (6), 4405-4410.

58. Bai, S.; Wang, X.; Hu, C.; Xie, M.; Jiang, J.; Xiong, Y., Two-dimensional g-C3N4: an ideal platform for examining facet selectivity of metal co-catalysts in photocatalysis. *Chem. Commun.* **2014,** *50* (46), 6094-6097.

59. Dong, G.; Zhang, L., Porous structure dependent photoreactivity of graphitic carbon nitride under visible light. *J. Mater. Chem.* **2012,** *22* (3), 1160-1166.

60. Xu, J.; Wang, Y.; Zhu, Y., Nanoporous Graphitic Carbon Nitride with Enhanced Photocatalytic Performance. *Langmuir* **2013,** *29* (33), 10566-10572.

61. Yang, S.; Gong, Y.; Zhang, J.; Zhan, L.; Ma, L.; Fang, Z.; Vajtai, R.; Wang, X.; Ajayan, P. M., Exfoliated Graphitic Carbon Nitride Nanosheets as Efficient Catalysts for Hydrogen Evolution Under Visible Light. *Adv. Mater.* **2013,** *25* (17), 2452-2456.

62. Niu, P.; Zhang, L.; Liu, G.; Cheng, H.-M., Graphene-Like Carbon Nitride Nanosheets for Improved Photocatalytic Activities. *Adv. Funct. Mater.* **2012,** *22* (22), 4763-4770.

63. Bai, X.; Wang, L.; Zong, R.; Zhu, Y., Photocatalytic Activity Enhanced via g-C3N4 Nanoplates to Nanorods. *J. Phys. Chem. C* **2013,** *117* (19), 9952-9961.

64. Zeng, Z.; Li, K.; Yan, L.; Dai, Y.; Guo, H.; Huo, M.; Guo, Y., Fabrication of carbon nitride nanotubes by a simple water-induced morphological transformation process and their efficient visible-light photocatalytic activity. *RSC Adv.* **2014,** *4* (103), 59513-59518.

65. Gu, Q.; Liao, Y.; Yin, L.; Long, J.; Wang, X.; Xue, C., Template-free synthesis of porous graphitic carbon nitride microspheres for enhanced photocatalytic hydrogen generation with high stability. *Applied Catalysis B-Environmental* **2015,** *165*, 503-510.

66. Tian, J.; Liu, Q.; Asiri, A. M.; Sun, X.; He, Y., Ultrathin graphitic C3N4 nanofibers: Hydrolysis-driven top-down rapid synthesis and application as a novel fluorosensor for rapid, sensitive, and selective detection of Fe3+. *Sensors and Actuators B-Chemical* **2015,** *216*, 453-460.